Drug Delivery

International Edition: DOI: 10.1002/anie.201506262
German Edition: DOI: 10.1002/ange.201506262

Transformable Peptide Nanocarriers for Expeditious Drug Release and Effective Cancer Therapy via Cancer-Associated Fibroblast Activation

*Tianjiao Ji[+], Ying Zhao[+], Yanping Ding[+], Jing Wang, Ruifang Zhao, Jiayan Lang, Hao Qin, Xiaoman Liu, Jian Shi, Ning Tao, Zhihai Qin, Guangjun Nie, and Yuliang Zhao**

Abstract: *A novel cleavable amphiphilic peptide (CAP) was designed to be specifically responsive to fibroblast activation protein-α (FAP-α), a protease specifically expressed on the surface of cancer-associated fibroblasts. The CAP self-assembled into fiber-like nanostructures in solution, while the presence of hydrophobic chemotherapeutic drugs readily transformed the assemblies into drug-loaded spherical nanoparticles. The disassembly of these nanoparticles (CAP-NPs) upon FAP-α cleavage resulted in rapid and efficient release of the encapsulated drugs specifically at tumor sites. This Transformers-like drug delivery strategy could allow them to disrupt the stromal barrier and enhance local drug accumulation. Therapeutic results suggested that drug-loaded CAP-NPs hold promising tumor specificity and therapeutic efficacy for various solid tumor models, confirming its potential utility and versatility in antitumor therapy.*

Nanomaterial-based drug delivery systems have long been seen as particularly promising for cancer therapy because of their great potential for improving drug specificity, biocompatibility, pharmacokinetic features, and antitumor efficacy.[1] However, for most particulate-based drug carriers, the heterogeneity among tumor cells and the presence of complex stromal cell barriers are still great challenges limiting their tumor-targeting and -penetrating performances,[2,3] and strategies to overcome tumor heterogeneity and to break stromal barriers are urgently needed.[2,4] Cancer-associated fibroblasts (CAFs), the predominant cell type in the tumor stroma,[5] form a major barrier that impedes penetration of nanoparticulate therapeutics and even molecular drugs into solid tumors.[6] Compared to tumor cells that show diverse marker proteins among different tumor types, CAFs selectively overexpressed certain proteins, such as α-smooth muscle actin (α-SMA) and fibroblast-activated protein-α (FAP-α), in almost all solid tumors but not normal tissues.[5,7,8] Consequently, development of smart nanomaterials responding to CAFs may be a specific and efficient strategy to overcome the aforementioned obstacles, leading to increased drug perfusion and improved antitumor efficacy.

Peptides and peptide derivatives, owing to their biocompatibility, chemical versatility, and biological recognition abilities, have been widely utilized as building blocks to construct soft functional biomaterials for specific applications, such as tissue engineering and drug delivery.[9] Extensive studies have demonstrated that tailor-made peptides can self-assemble into unique secondary structures or nanostructures.[10] Moreover, certain peptides derived from degradation or cleavage of antibodies or collagens exhibit specific targeting capacity and enzymatic activity.[11] These features render peptides extremely useful in the construction of versatile, multi-functional, and stimuli-responsive nanostructures for drug delivery and release,[12] especially in tumor tissues overexpressing proteases.

Herein we report a novel CAF-targeting drug delivery nanosystem based on a cleavable amphiphilic peptide (CAP) designed to be specifically responsive to FAP-α, a membrane-bound serine protease specifically expressed on CAFs.[13] In aqueous solution, CAP monomers readily self-assembled into nanofibers because of their amphiphilicity, which would transform into spherical nanoparticles (NPs) upon encapsulation of hydrophobic drugs. When entered into tumor stroma, the CAP molecules were cleaved by FAP-α, losing amphiphilicity and causing the NPs to rapidly disassemble, thereby discharging their cargoes. This stimulus-responsive nanocarrier is potentially applicable for the delivery of a broad spectrum of poorly soluble chemotherapeutic drugs, being able to greatly enhance tumor targeting and drug delivery efficacy. As FAP-α is specifically expressed and activated on CAFs in over 90% of human carcinomas,[8] a FAP-α-targeting drug delivery system can be particularly desirable in establishing an efficient treatment of a broad range of cancers.

The CAP monomer had a sequence of Ac-Ala-Thr-Lys(C18)-Asp-Ala-Thr-Gly-Pro-Ala-Lys(C18)-Thr-Ala-NH_2 and displayed a Gemini-like structure (Figure 1a).[14] Its hydrophilic domain contains the amino acid residue sequence Gly-Pro-Ala-X that can be specifically cleaved by FAP-α.[13,15] Three threonines (Thr) containing hydroxy groups were

[*] T. Ji,[+] Dr. Y. Zhao,[+] Dr. Y. Ding,[+] J. Wang, R. Zhao, J. Lang, H. Qin, J. Shi, Prof. Dr. G. Nie, Prof. Dr. Y. L. Zhao
CAS Key Laboratory for Biomedical Effects of Nanomaterials and Nanosafety
National Center for Nanoscience and Technology (NCNST)
11 Beiyitiao, Zhongguancun, Beijing 100190 (China)
E-mail: zhaoyl@nanoctr.cn
X. Liu, Dr. N. Tao, Prof. Dr. Z. Qin
CAS Key Laboratory of Protein and Peptide Pharmaceuticals, Institute of Biophysics
15 Datun Road, Beijing 100101 (China)
[+] These authors contributed equally to this work.

Supporting information for this article is available on the WWW under http://dx.doi.org/10.1002/anie.201506262.

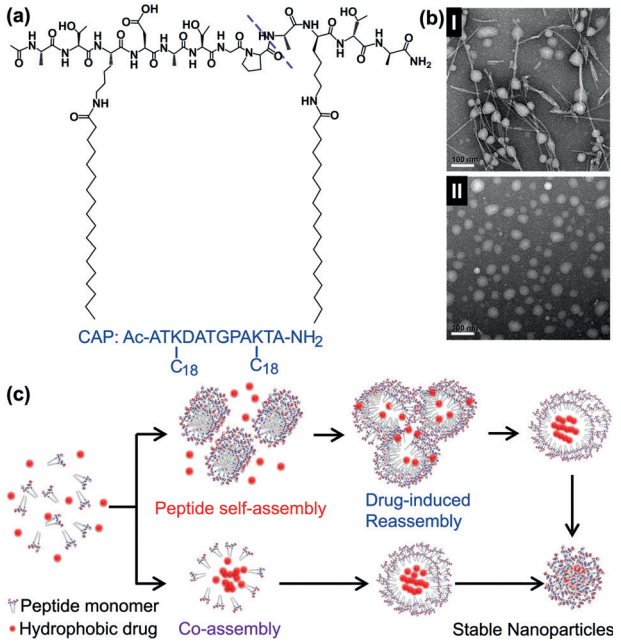

Figure 1. a) The structure of CAP. CAP contains a TGPA peptide sequence that can be cleaved by FAP-α (dashed line). b) Morphologies of peptide assemblies during Dox loading observed by TEM. The assembled product transforms from mace-like (I) to spherical (II) with prolonged ultrasonication. Scale bar: 100 nm. c) Proposed mechanisms of peptide self-assembly, drug induced reassembly and peptide and drug co-assembly in the hydrophobic drug and amphiphilic peptide mixed solution. Finally, they form the stable nanoparticles.

added into the hydrophilic domain to increase its hydrophilicity, and an aspartic acid (Asp) containing carboxyl group was incorporated to provide negative charges for the hydrophilic head at pH 7.4, to decrease nonspecific phagocytosis by the reticuloendothelial system (RES) and prolong blood circulation time in vivo.[16,17] The N-terminus was protected with acetyl (Ac) to avoid undesirable cleavage by the lymphatic vessel-expressed protease, dipeptidyl peptidase IV (DPPIV), which shares the same substrates with FAP-α but is unable to cleave N-terminus blocked peptides.[18] Furthermore, two octadecanoic acid chains were linked to the side-chains of the lysine residues of CAP to form the hydrophobic domain. We also synthesized an un-cleavable amphiphilic peptide (UAP) (Supporting Information, Figure S1a) with a similar structure and sequence of CAP as a control. The purity of CAP and UAP was over 95% (Figure S1b,S1c). The responsiveness of CAP and UAP towards FAP-α and DPPIV was detected by matrix-assisted laser desorption ionization time of flight mass spectrometry (MALDI-TOF MS) (Figure S2). After incubation with FAP-α for 3 h, the peak of CAP ($M = 1705$) disappeared with the emergence of two fragment peaks ($M1 = 655$, $M2 = 1068$), which correspond to the two predicted digested segments: Ac-Ala-Lys(C18)-Asp-Ala-Thr-Gly-Pro-OH and Ala-Lys(C18)-Thr-Ala-NH_2. When CAP was incubated with DPPIV, the peak $M = 1705$ remained and no other peaks emerged, indicating that CAP cannot be cleaved by the non-tumor related enzyme DPPIV. As expected, UAP exhibited no responsiveness towards either FAP-α or DPPIV. Both CAP and UAP have low critical micelle concentration (CMC) (CAP, 0.66 μM; UAP, 0.89 μM) in PBS buffer (Figure S3), implying that they are able to self-assemble into core-shell structures at concentrations equal to or above the CMC.

The drug loading capacity of CAP was first studied with the hydrophobic drug doxorubicin (Dox). Dox and CAP were dissolved in dimethyl sulfoxide and then diluted in water. After being ultrasonicated for 3 min and further incubated for 1 h, the product exhibited a mixture of multi-shaped nanostructures, including nanofibers, spherical NPs and mace-like structures, as demonstrated by transmission electron microscopy (TEM) measurements (Figure 1b,I). However, the assembled product transformed into uniform NPs after prolonged ultrasonication (Figure 1b,II). Thus, we hypothesize that the encapsulation of drugs by amphiphilic peptides may involve three processes (Figure 1c): peptide self-assembly into fiber-like structures, co-assembly of hydrophobic Dox and peptides into spherical NPs, and Dox-induced reassembly of nanofiber into NPs.

Further investigation was then carried out on the self-assembly behavior of engineered amphiphilic peptides. According to Israelachvili's surfactant number theory,[19,20] both the CAP and UAP monomers have a dimensionless packing parameter P ($P = v/al$; where v = volume of hydrophobic tail, a = area of hydrophilic head group, and l = monomer length) between 0.5 and 1 because of their short hydrophilic domains yet long hydrophobic tails (CAP, $P = 0.58$; UAP, $P = 0.56$), which predicts a tendency to form fiber-shaped micelles during self-assembly. This was confirmed by TEM analysis that showed that in the absence of Dox, CAP dynamically self-assembled into well-ordered, thin nanofibers (Figure 2a). Morphologies of intermediate products suggested a possible multi-phased mechanism of CAP self-assembly (Figure S4a). Initially, disordered peptide monomers assembled into loose peptide aggregates (transient state I), driven by both the hydrophobic interactions among alkyl chains and intermolecular hydrogen bonds formed between amide groups. The alkyl chains were then driven closer, expelling water out of the aggregates and causing them

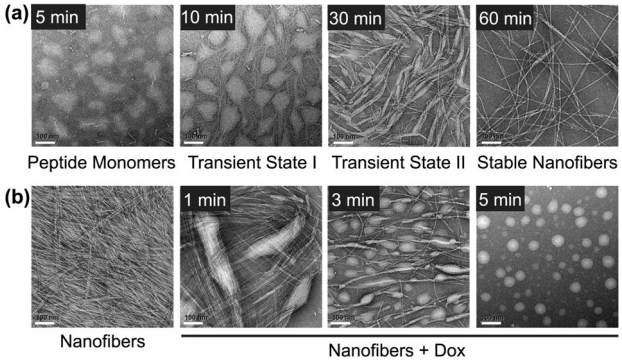

Figure 2. a) Self-assembly process of CAP analyzed by TEM. CAP concentration, 0.05 mg mL^{-1}. b) TEM examination of morphology changes of peptide nanocarriers during loading of hydrophobic Dox. Scale bars: 100 nm.

to gradually shrink, which leads to the transformation of the aggregates to long and thin fiber-like structures with water completely expelled from the hydrophobic core (transient state II). Finally, the resulting nanofibers were dispersed, capable of forming stable structures owing to their negatively charged surfaces, provided by the Asp carboxyl group side chains. The UAP had a similar self-assembly process with CAP (Figure S4b). The height of these nanofibers, as measured by atomic force microscope (AFM), was approximately 4 nm (Figure S5), confirming the formation of nanofibers by a monolayer of CAP molecules.

However, when Dox was added into the system, the assembled product changed from nanofibers to nanospheres. It is easy to imagine that amphiphilic peptide monomers could directly encapsulate the drug through a one-step co-assembly process, where hydrophobic drug molecules form the hydrophobic cores that induce the alkyl chains of peptide to assemble around them (Figure 1c). Nonetheless, since self-assembly of peptide and co-assembly of peptide and drug simultaneously occurred during drug loading, a reassembly of the self-assembled peptide nanofibers upon interaction with the drug was probably involved. To exploit the reassembly process, diverse small molecular weight hydrophobic drugs were incubated with CAP in aqueous solution under ultrasonication for different time intervals and the morphologies of the assembled products were observed. After co-incubation of CAP with Dox for 1 min, silkworm cocoon-like structures emerged among nanofibers (Figure 2b). When the ultrasonication time was increased to 3 min, the amount of nanofibers significantly decreased and many spherical particles appeared. After 5 min or longer ultrasonication time, nanofibers disappeared and were ultimately transformed to spherical NPs. The morphology of the NPs was unchanged even after incubation with serum for 48 h (Figure S6), indicating their high stability under physiological conditions. Substituting Dox with two other first-line chemotherapeutic drugs, irinotecan (Iri) and paclitaxol (Tax), also elicited similar morphological changes during the drug loading process, except that longer ultrasonication was needed in their cases to form the spherical structures (Figure S7), which may be due to different physiochemical properties of these hydrophobic drugs. On the other hand, without hydrophobic drugs, the nanofibers did not change their shape even after longer time of ultrasonication (Figure S7), suggesting that hydrophobic drugs are necessary to the described morphological transformation. These observations are consistent with the proposed mechanism of the drug-induced reassembly process (Figure 1c): ultrasonication increased the collision between hydrophobic drug molecules and nanofibers, during which the drug molecules inserted into the inner hydrophobic part of these fibers, forming hydrophobic cores. These drug-incorporated cores induced the rearrangement of surrounding peptide monomers through the hydrophobic driving force, resulting in the transformation into stable spherical NPs.

Taken together, these data indicate that we have successfully constructed a nanocarrier for delivery of hydrophobic drugs using a FAP-α responsive peptide CAP. With proper size (sub-100 nm; Table S1), zeta potential (negative charges, Table S1), capacity of encapsulating hydrophobic drugs

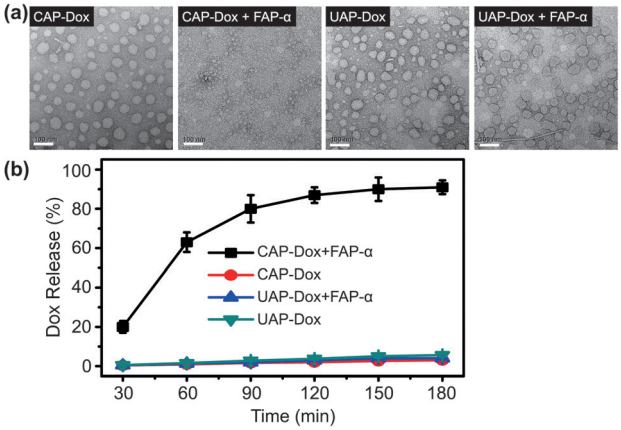

Figure 3. a) Morphology changes of peptide nanocarriers upon reaction with FAP-α (TEM). Scale bar: 100 nm. b) The drug release profiles of CAP-Dox and UAP-Dox in the presence or absence of FAP-α.

(Table S2), as well as specific responsiveness to CAFs, these drug-peptide complexes hold great potential to be used for antitumor therapy.

Efficient and specific drug release is considered essential for a drug delivery nanosystem to achieve high therapeutic efficacy. In our study, we found that FAP-α was able to completely dissociate Dox-loaded CAP NPs (CAP-Dox) into disordered structures, but had no effect on the morphology of Dox-loaded UAP NPs (UAP-Dox) (Figure 3a). Without FAP-α, both CAP-Dox and UAP-Dox released Dox at similarly low rates (less than 40% in 48 h) (Figure S8). In contrast, CAP-Dox released almost all loaded drugs within 3 h after FAP-α treatment, while UAP-Dox maintained the slow Dox release rate (Figure 3b). This rapid drug release behavior of CAP-Dox in response to FAP-α was attributed to FAP-α triggered CAP cleavage, resulting in two segments with unbalanced hydrophilicity and hydrophobicity (Figure S9). These structures are unable to maintain a stable assembly or reassembly status. With rapid and efficient enzymatic response, our nanosystem is expected to greatly increase the effective drug concentration at the FAP-α-rich tumor sites, thus enhancing drug delivery/perfusion.

Most nanostructures with negative surface charge have been reported to suffer low cellular uptake.[21] To investigate the interaction between our drug-loading nanosystem and cells in vitro, we first incubated CAP-Dox or UAP-Dox with CAFs, PC-3 (a prostate cancer cell line) or human umbilical endothelial cells (HUVECs), and assessed the cellular uptake of encapsulated Dox (Figure S10). Results showed that after CAP-Dox treatment for 4 h, CAFs with high expression of FAP-α exhibited a pronounced intracellular Dox signal while only a small amount of Dox signal was observed in the FAP-α negative cell lines, PC-3 and HUVEC (Figure S11). Even after incubation for 24 h, the Dox signal was still very weak in PC-3 and HUVECs while most of the CAFs had been killed (Figure S10). In comparison, all three types of cells only showed minimal Dox signal when treated with UAP-Dox, likely due to the lack of a cleavage site for FAP-α in UAP. These results are consistent with the difference between drug release profiles of the two NPs, suggesting that the high drug

release efficiency of CAP-Dox would result in increased cellular uptake of drugs. Importantly, when examined by cytotoxicity assays, CAP-Dox showed specific and dose-dependent cytotoxicity to CAFs and no significant toxicity to either PC-3 or HUVECs (Figure S12), confirming the specificity of FAP-α responsive Dox release from CAP-Dox. As expected, UAP-Dox had no observable toxicity to any of the three cell types. We next used a co-culture system (CAFs + PC-3 cells) to simulate a tumor environment enriched with CAFs in vitro (Figure S13). After CAP-Dox treatment for 4 h, a significant cellular uptake of Dox was observed in both cell types. In contrast, little Dox uptake was detected in UAP-Dox treated cells. These results imply that other than selective drug release at CAF-present tumor sites to avoid off-target effects, the specific response of CAP-Dox to FAP-α also allows the released Dox to act on not only CAFs but also the co-existing tumor cells.

Subsequently, we assessed the tumor targeting and biodistribution of engineered nanocarrier in vivo. Tetramethylrhodamine isothiocyanate (TRITC) and Black Hole Quencher (BHQ-1) were encapsulated in CAP, fabricating a nanoprobe (CAP-RB, Figure S14),[22] which can be activated by FAP-α. The in vivo imaging indicated that the tailor-made peptide nanocarrier specifically released its cargoes at the tumor site in the CAF-rich tumor model (Figure 4a). The biodistribution results illustrated that CAP NPs possessed not only excellent tumor specificity but also low non-specific organ accumulation (Figures S15, S16).

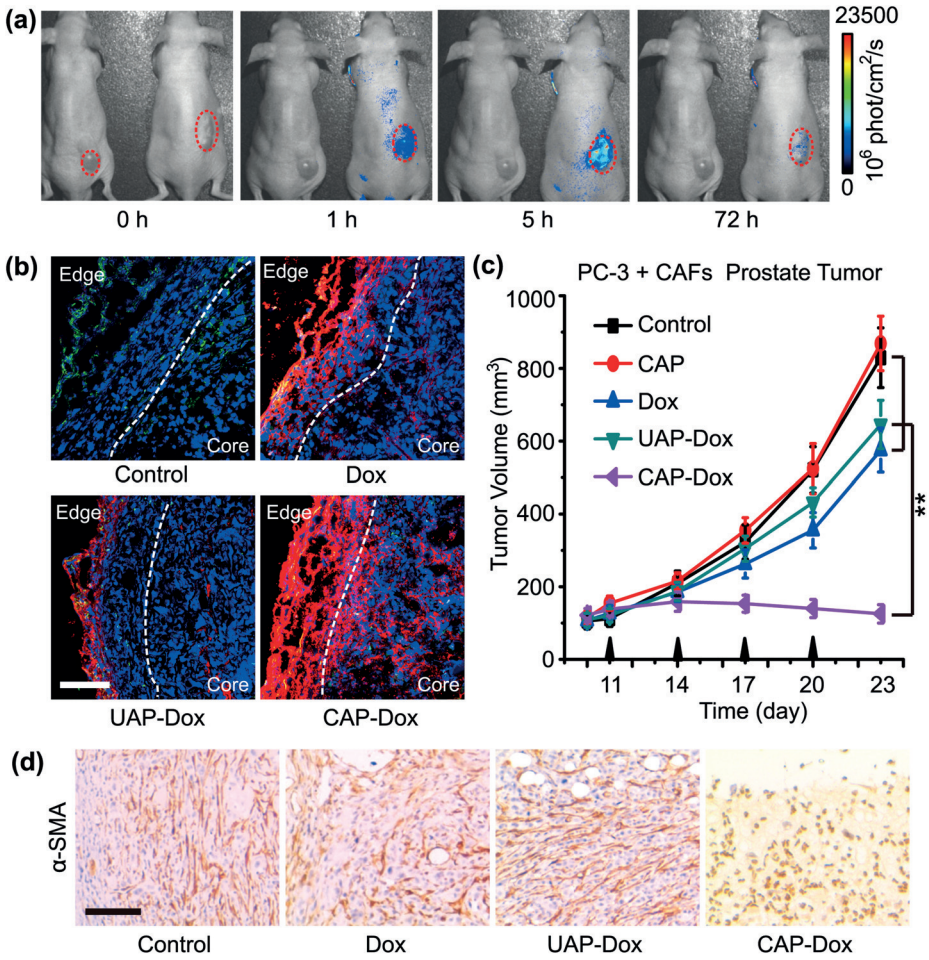

Figure 4. a) In vivo imaging of CAP-RB after intravenous injection into mice bearing CAFs and PC-3 co-implants. The fluorescence signal emerged at the tumor site within 1 h after intravenous injection of CAP-RB and reached its maximum at 5 h post-injection. The signal gradually decreased to undetectable levels after 72 h. b) Penetration of Dox into prostate tumor (PC-3 and CAF co-implanted) tissues after intravenous injection of different Dox formulations. Frozen tumor sections were stained with DAPI (blue) to label nuclei and CD31 (green) antibody to label tumor vasculature. Red: Dox. Scale bar: 100 μm. c) The growth curves of PC-3 and CAF co-implanted prostate tumors in mice treated by different Dox formulations. Data are presented as mean ± S.D. ($n = 8$). **$p < 0.01$ vs. control, Dox and UAP-Dox groups. d) Immunochemical staining of α-SMA in tumor slices from the indicated formulation treated groups. Scale bar: 50 μm.

Drug delivery efficiency of the CAP nanocarriers to tumors was investigated by intravenous injection of free Dox, CAP-Dox and UAP-Dox (the same Dox dose, 5 mg kg^{-1}, was used in all formulations) into mice bearing CAFs and PC-3 co-implants. After 24 h post-injection, tumors were resected and sectioned, and the tumor blood vessels were labeled with CD31 antibody. Confocal microscopy images showed a gradient of Dox fluorescence from the tumor edge to the core that was much wider and stronger in CAP-Dox-treated tumors compared to either UAP-Dox or free Dox-treated groups (Figure 4b, Figure S17). Although free Dox also exhibited a degree of diffusion into tumors, its penetration distance was much shorter than that of CAP-Dox, as demonstrated by the fluorescence distribution across the tumor tissue. This was probably caused by the low tumor targeting efficiency of Dox together with the drug expelling effect of high interstitial pressure. In UAP-Dox treated tumors, fluorescence of Dox was detectable only at the tumor edge and with very low intensity, because of inefficient drug release and poor penetration through the stromal barrier.

Having confirmed the capacity of CAP-Dox to effectively release drugs and enhance drug delivery to tumors, we further examined its antitumor therapeutic efficacy. Mice were co-inoculated with CAFs and PC-3 cells to establish a xenograft prostate tumor model with enriched CAFs. When tumors reached an average volume of 100 mm^3, the mice were randomly divided into five groups ($n = 8$) and intravenously injected with PBS (control), CAP, Dox, CAP-Dox, or UAP-

Dox every three days (5 mg kg^{-1} Dox per injection). Tumor volumes were measured and calculated post treatment (Figure 4c). CAP-Dox significantly inhibited tumor growth after only two injections and gradually reduced tumor volume with subsequent treatment, exhibiting much superior antitumor effects to free Dox. In comparison, tumor growth in the UAP-Dox-treated group was only slightly suppressed. After four injections, tumor tissues were resected and subjected to H&E staining, immunohistochemistry (IHC) analysis of CAFs by labeling α-SMA,[23] and terminal deoxynucleotidyl transferase dUTP nick end labeling (TUNEL) staining for apoptosis (Figure 4d and Figure S18). Compared to the control group, free Dox and UAP-Dox only showed a mild antitumor activity, both eliciting little change in tumor morphology, limited reduction of CAFs and no apparent apoptosis. In contrast, the morphology of tumors in the CAP-Dox-treated group dramatically changed, with most cells in an apoptotic state. Furthermore, the typical morphology of CAFs disappeared after CAP-Dox treatment (Figure S18 and Figure 4d). The percentage of apoptotic cells determined in each group also supported the above observations (Figure S18), as the TUNEL-positive cells in CAP-Dox treated tumors had a percentage about 65 ± 6.8%, much higher than those in other groups (control, 7 ± 2%; Dox, 18 ± 3.4%; UAP-Dox, 11 ± 2.5%). These results suggest that the CAP-Dox nanosystem selectively and effectively respond to CAFs for drug release, and demonstrate promising antitumor efficacy.

Considering the cardiotoxicity of Dox and the distribution of CAP-NPs in liver and kidney for a certain period,[24] in vivo side effects of the peptide nanocarrier were evaluated (Figure S19). The control group showed a small degree of morphological differences, with only the liver showing some apoptotic areas. However, no obvious morphological changes were observed in the UAP-Dox or CAP-Dox treated groups, indicating the minimal side effects of our designed peptide nanocarrier.

We further identified the versatility of the CAP nanosystem in another two xenograft tumor models, MCF-7 breast tumor and Mia-paca-2 pancreatic tumor. Although both tumor cell lines were FAP-α negative, they ultimately formed tumors that exhibited positive FAP-α expression (Figure S20), indicating the presence of CAFs in the tumor microenvironment. When we used CAP nanoparticles loaded with Tax or Iri to treat breast or pancreatic tumors, respectively, tumor growth was almost completely inhibited. The antitumor efficiency of CAP-NPs was much higher than that of UAP-NPs or free drug (Figure S21). These data further suggest that our CAP nanocarrier is of great potential for treatment of a wide range of solid tumors that contain or recruit FAP-α positive CAFs. Furthermore, the stability and responsive properties of CAP-NPs in blood (Figure S22) imply the potential opportunity to apply CAP-NPs in clinical cancer therapy.

In summary, using the self-assembly properties of a designed amphiphilic peptide, we developed a smart Transformers-like drug delivery system based on a cleavable amphiphilic peptide that specifically responded to FAP-α expressed on CAFs in the tumor microenvironment, achieving enhanced drug delivery and promising antitumor effects. The nanocarrier exhibited an interesting morphological transformation during the loading of hydrophobic drugs, and was able to rapidly disassemble upon cleavage by FAP-α to release the drug, facilitating drug penetration into the tumor microenvironment. In vivo fluorescence imaging showed that the CAP nanocarrier possesses excellent tumor targeting specificity, which significantly reduced the side effects of the encapsulated chemotherapeutics on normal tissues. We believe that our study demonstrated the potential utility of tumor microenvironment-responsive drug delivery nanosystems in enhancing both specific delivery and tumor penetration for antitumor therapy.

Experimental Section

All animal experiments were carried out in accordance with the national animal guidelines. Detailed experimental procedures for the synthesis and characterizations of CAP-NPs and UAP-NPs, morphologies from TEM and AFM, cell culture, tumor histology, toxicity evaluation, and therapeutic efficacy in breast and pancreatic tumor models are available in Supporting Information.

Acknowledgements

The authors thank Professor Ju Zhang from Nankai University for providing PF179T-CAF cell line. This work was supported by the grants from MOST 973 (2012CB934004, 2011CB933400, and 2013CB932701), the NSFC (21320102003, 31170962, 51203032, 21373067, 31300822), and the Key Research Program of the Chinese Academy of Sciences, Grant No. KGZD-EW-T06. G.N. acknowledges the support from National Distinguished Young Scientists grant (31325010).

Keywords: cancer-associated fibroblasts · drug delivery · fibroblast activation protein-α · morphological transformation · peptide assembly

How to cite: *Angew. Chem. Int. Ed.* **2016**, *55*, 1050–1055
Angew. Chem. **2016**, *128*, 1062–1067

[1] a) T. Sun, Y. S. Zhang, B. Pang, D. C. Hyun, M. Yang, Y. Xia, *Angew. Chem. Int. Ed.* **2014**, *53*, 12320–12364; *Angew. Chem.* **2014**, *126*, 12520–12568; b) T. Ji, Y. Zhao, Y. Ding, G. Nie, *Adv. Mater.* **2013**, *25*, 3508–3525.
[2] T. A. Denison, Y. H. Bae, *J. Controlled Release* **2012**, *164*, 187–191.
[3] V. P. Chauhan, R. K. Jain, *Nat. Mater.* **2013**, *12*, 958–962.
[4] D. Ling, M. J. Hackett, T. Hyeon, *Nat. Mater.* **2014**, *13*, 122–124.
[5] a) N. A. Bhowmick, E. G. Neilson, H. L. Moses, *Nature* **2004**, *432*, 332–337; b) R. Kalluri, M. Zeisberg, *Nat. Rev. Cancer* **2006**, *6*, 392–401.
[6] a) S. M. Sagnella, J. A. McCarroll, M. Kavallaris, *Nanomed-Nanotechnol.* **2014**, *10*, 1131–1137; b) T. Stylianopoulos, J. D. Martin, V. P. Chauhan, S. R. Jain, B. Diop-Frimpong, N. Bardeesy, B. L. Smith, C. R. Ferrone, F. J. Hornicek, Y. Boucher, L. L. Munn, R. K. Jain, *Proc. Natl. Acad. Sci. USA* **2012**, *109*, 15101–15108.
[7] O. E. Franco, A. K. Shaw, D. W. Strand, S. W. Hayward, *Semin. Cell Dev. Biol.* **2010**, *21*, 33–39.

[8] a) K. Räsänen, A. Vaheri, *Exp. Cell Res.* **2010**, *316*, 2713 – 2722; b) P. O'Brien, B. F. O'Connor, *Biochim. Biophys. Acta Proteins Proteomics* **2008**, *1784*, 1130 – 1145.
[9] a) J. Kopeček, J. Yang, *Angew. Chem. Int. Ed.* **2012**, *51*, 7396 – 7417; *Angew. Chem.* **2012**, *124*, 7512 – 7535; b) T. Dvir, B. P. Timko, D. S. Kohane, R. Langer, *Nat. Nanotechnol.* **2011**, *6*, 1748 – 3387; c) T. J. Moyer, J. A. Finbloom, F. Chen, D. J. Toft, V. L. Cryns, S. I. Stupp, *J. Am. Chem. Soc.* **2014**, *136*, 14746 – 14752.
[10] a) C. L. Chen, N. L. Rosi, *Angew. Chem. Int. Ed.* **2010**, *49*, 1924 – 1942; *Angew. Chem.* **2010**, *122*, 1968 – 1986; b) L. Adler-Abramovich, D. Aronov, P. Beker, M. Yevnin, S. Stempler, L. Buzhansky, G. Rosenman, E. Gazit, *Nat. Nanotechnol.* **2009**, *4*, 849 – 854; c) E. F. Banwell, E. S. Abelardo, D. J. Adams, M. A. Birchall, A. Corrigan, A. M. Donald, M. Kirkland, L. C. Serpell, M. F. Butler, D. N. Woolfson, *Nat. Mater.* **2009**, *8*, 596 – 600.
[11] a) V. R. Elena, E. K. Jacob, G. R. Corban, B. P. Niranjan, P. T. Amir, S. P. Aleksander, *Curr. Pharm. Biotechnol.* **2011**, *12*, 1101 – 1116; b) M. Tihomir, L. M. Nicole, E. M. G. Peter, T. Cicerone, K. H. Fred, D. M. Mahin, *J. Biol. Chem.* **2012**, *287*, 24698 – 24712.
[12] a) Z. Zhao, H. Meng, N. Wang, M. J. Donvan, T. Fu, M. You, Z. Chen, X. Zhang, W. Tan, *Angew. Chem. Int. Ed.* **2013**, *52*, 7487 – 7491; *Angew. Chem.* **2013**, *125*, 7635 – 7639; b) X. X. Zhang, H. S. Eden, X. Chen, *J. Controlled Release* **2012**, *159*, 2 – 13.
[13] a) J. E. Park, M. C. Lenter, R. N. Zimmermann, P. Garin-Chesa, *J. Biol. Chem.* **1999**, *274*, 36505 – 36512; b) O. Abbas, J. E. Richards, M. Mahalingam, *Mod. Pathol.* **2010**, *23*, 1535 – 1543.
[14] F. M. Menger, C. A. Littau, *J. Am. Chem. Soc.* **1993**, *115*, 10083 – 10090.
[15] a) S. Aggarwal, W. N. Brennen, T. P. Kole, E. Schneider, O. Topaloglu, M. Yates, R. J. Cotter, S. R. Denmeade, *Biochemistry* **2008**, *47*, 1076 – 1086; b) J. D. Cheng, L. M. Weiner, *Clin. Cancer Res.* **2003**, *9*, 1590 – 1595.
[16] A. N. Ilinskaya, M. A. Dobrovolskaia, *Nanomedicine* **2013**, *8*, 969 – 981.
[17] M. Ekkapongpisit, A. Giovia, C. Follo, G. Caputo, C. Isidoro, *Int. J. Nanomed.* **2012**, *7*, 4147 – 4158.
[18] a) K. Aertgeerts, I. Levin, L. Shi, G. P. Snell, A. Jennings, G. S. Prasad, Y. Zhang, M. L. Kraus, S. Salakian, V. Sridhar, R. Wijnands, M. G. Tennant, *J. Biol. Chem.* **2005**, *280*, 19441 – 19444; b) A. M. LeBeau, W. N. Brennen, S. Aggarwal, S. R. Denmeade, *Mol. Cancer Ther.* **2009**, *8*, 1378 – 1386.
[19] J. Israelachvili, *Intermolecular and Surface Forces*, Elsevier, London, **2011**, pp. 535 – 576.
[20] A. Trent, R. Marullo, B. Lin, M. Black, M. Tirrell, *Soft Matter* **2011**, *7*, 9572 – 9582.
[21] a) Z. Poon, J. B. Lee, S. W. Morton, P. T. Hammond, *Nano Lett.* **2011**, *11*, 2096 – 2103; b) E. Fröhlich, *Int. J. Nanomed.* **2012**, *7*, 5577 – 5591.
[22] J. Y. Ko, S. Park, H. Lee, H. Koo, M. S. Kim, K. Choi, I. C. Kwon, S. Y. Jeong, K. Kim, D. S. Lee, *Small* **2010**, *6*, 2539 – 2544.
[23] a) S. E. Holton, M. J. Walsh, A. Kajdacsy-Balla, R. Bhargava, *Biophys. J.* **2011**, *101*, 1513 – 1521; b) M. Bauer, G. Su, C. Casper, R. He, W. Rehrauer, A. Friedl, *Oncogene* **2010**, *29*, 1732 – 1740.
[24] Y. W. Zhang, J. Shi, Y. J. Li, L. Wei, *Arch. Immunol. Ther. Exp.* **2009**, *57*, 435 – 445.

Received: July 7, 2015
Published online: August 17, 2015

